Bicontinuous Nanoporous Polymers by Carbon Dioxide Foaming

B. Krause, H. J. P. Sijbesma, P. Münüklü, N. F. A. van der Vegt,* and M. Wessling

Membrane Technology Group, University of Twente, P.O. Box 217, 7500 AE Enschede, The Netherlands

Received May 16, 2001; Revised Manuscript Received September 20, 2001

ABSTRACT: We investigate the physical foaming process of glassy poly(ether imide) and poly(ether sulfone) using carbon dioxide and report temperature−concentration diagrams ("foam diagrams") marking out the foaming envelope in which dense CO_2-saturated films expand and microvoids are introduced. Two types of porosities are observed. Closed microcellular structures occur at carbon dioxide saturation levels below 50 cm³ (STP)/cm³ (polymer); nanoporous bicontinuous (open) structures with pore sizes as small as 40 nm occur above this CO_2 concentration threshold, which is identical for both polymers. The cellular-to-bicontinuous transition is characterized in detail on the basis of gas permeation measurements and is represented as a separate window inside the foaming diagram. In this paper, the transition to bicontinuous structures is reported for the first time, and its generic physical basis is critically reviewed.

1. Introduction

Foaming of polymers using environmentally friendly physical blowing agents in their supercritical or non-supercritical state has become of significant interest in the past decades. An overview about the foaming of glassy polymers using carbon dioxide is given by Kazarian.[1] Different continuous and discontinuous process variants[1−3] have been developed to prepare microcellular (cell diameter between 1 and 10 μm) foam morphologies from glassy polymers. All these techniques rely on the same principle: (1) the polymer is saturated with a gaseous penetrant (blowing agent) at high pressure, (2) the polymer/gas mixture is quenched into a supersaturated state by either reducing pressure or increasing temperature, and (3) nucleation and growth of gas cells dispersed throughout the polymer sample evolves until all thermodynamic forces driving mass transport vanish.

Mainly amorphous and semicrystalline glassy commodity polymers such as poly(vinyl chloride),[2] polystyrene,[4−6] polycarbonate,[7,8] poly(methyl methacrylate),[8−11] poly(ethylene terephthalate),[12,13] and some block copolymers[14−16] were investigated using different foaming techniques and applying carbon dioxide as blowing agent. The foams obtained in each of these investigations exhibit closed cell structures with sample dimensions in the range of several micrometers. Such closed cell microcellular materials find applications as packaging, construction, and insulation materials.[17,18] However, for several other applications such as food packaging, controlled release systems, bone substitute materials, and membranes for liquid separations, interconnected porous materials (open cell foams) are required.

Until now, foamed polymeric materials with an interconnected porous structure and tailored mass transport properties have not been subject of extensive studies. Huang[19,20] presented an extrusion process to prepare foamed hollow fibers with relatively large cells of approximately 10 μm in diameter. The presented SEM micrographs did not provide a direct proof of interconnected cells; however, the gas permeation data

presented did prove some extent of openness. Rodeheaver[21] presented results on foaming of polystyrene using nitrogen as blowing agent and used mercury porosimetry to analyze the interconnectivity of cells. The use of mercury porosimetry to determine pore sizes smaller than 100 nm in polymeric materials is difficult due to the enormous pressures (>75 bar) required. No alternative characterizations were reported by the author to demonstrate open cells. Krause et al.[22] studied cellular polysulfone foams and applied trace (0.02−0.8 wt %) concentrations of tetrahydrofuran to achieve cell openings. Scanning electron microscopy and helium permeation was used to demonstrate cell openings and substantiate the openness of the samples.
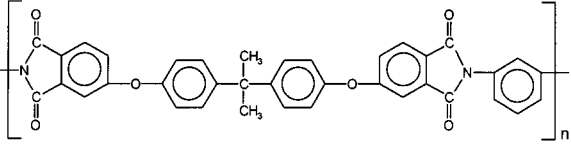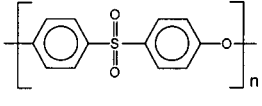
In this work, we study the foaming behavior of thin (∼75 μm) extruded poly(ether imide) (PEI) and poly-(ether sulfone) (PES) films using the discontinuous solid-state microcellular foaming process[2,3] with carbon dioxide as blowing agent. It is our purpose to present temperature−concentration diagrams ("foam diagrams") marking out the regions (foaming envelope) where a CO_2-saturated polymer/gas mixture changes into a cellular structure. In particular, we report the discovery of a critical carbon dioxide content of the mixture above which closed-cellular morphologies no longer develop. Instead, nanoporous bicontinuous (open) foams are found within a temperature−concentration window, which we locate by means of gas permeation measurements.

The foaming envelope is bounded by a lower (T_{lower}) and an upper temperature (T_{upper}), which we discussed in detail in a previous paper.[3] The lower temperature is the glass transition temperature, $T_g(c)$, of the polymer/gas mixture at CO_2 concentration c. The upper temperature ($T_{upper} > T_g(0)$) occurs due to carbon dioxide loss (diffusion) from the sample and thus depends on the film dimensions and the foaming time. In this paper we closely examine cell diameters, cell densities, and foam morphologies at different points in the foaming window. Moreover, we show that at points close to $T_g(c)$ the extent of film expansion is determined by the distance from the glass transition ($T - T_g(c)$).

In section 2 we describe the experimental details. In section 3.1 the foam diagrams of PES and PEI are

* Corresponding author: e-mail n.f.a.vandervegt@ct.utwente.nl.

Table 1. Chemical Structure, Mass Density, Glass Transition Temperature, and Dual-Mode Sorption Parameters of CO_2 for the PEI and PES Films at 25 °C

	Polyetherimide	Polyethersulfone
Chemical structure of the monomer units		
T_g, °C	218	230
Mass density, g/cm^3	1.28	1.36
k_D, cm^3(STP)/cm^3 (polymer)/bar	0.428	0.265
C'_H, cm^3(STP)/cm^3 (polymer)	40.01	45.11
b, bar^{-1}	0.088	0.126

introduced. Microcellular foam characteristics are presented in section 3.2. In section 3.3 the transition from cellular to bicontinuous structures is discussed, and helium flow measurements are presented to identify the (open) bicontinuous regions in the foam diagram. The innovative aspects of this investigation and our interpretation of the observed experimental results are presented in section 4.

2. Experimental Section

2.1. Materials. Two commercially available extruded polymer sheets were used during this investigation: (1) poly(ether imide), type Ultem 1000, received from GE Plastics B.V., The Netherlands, and (2) poly(ether sulfone), type Ultrason E, received from Westlake Plastics. The thickness of both polymer sheets was 75 μm, and they were free of additional plasticizer, filler, or any other kind of additives. The chemical structure of the two polymers is shown in Table 1. Glycerol, hexane, and ethanol were purchased from Merck (analytical grade) and used as received. Carbon dioxide was purchased from Praxair having purity a larger than 99.99%.

2.2. Polymer Film Characterization. Both polymer films were characterized to determine their glass transition temperature, mass density, and carbon dioxide sorption capacities. A Perkin-Elmer differential scanning calorimeter DSC7 was used to determine the glass transition temperature of the films. The T_g was obtained from the second heating run, using a heating rate of 20 K/min. The mass densities of the foamed polymer samples were analyzed by using the flotation weight loss method (ASTM D-792) with hexane as liquid. Hexane uptake in the foamed sample could not be observed during the measurement, which process would overestimate the true density.

The equilibrium sorption of carbon dioxide into the two polymer films was measured using a dual volume setup similar to the one described by Koros et al.[23,24] The equipment used and the experimental procedure of the sorption measurements is described elsewhere.[25] Sorption isotherms for the pressure range up to 50 bar at 25 °C were determined for both films. The obtained equilibrium data points were fitted by the dual-mode sorption model.[26] The dual-mode sorption parameters together with the measured T_g and mass density for both polymers are given in Table 1. Figure 1 shows the carbon dioxide sorption isotherms for the PES and PEI sheets at 25 °C.

2.3. Foam Formation Technique. The polymer films were cut into 4 cm × 4 cm pieces and placed in a pressure vessel connected to a carbon dioxide cylinder. The samples were then saturated with carbon dioxide at room temperature (25 °C) and elevated pressure (1−57 bar). Subsequently, the carbon
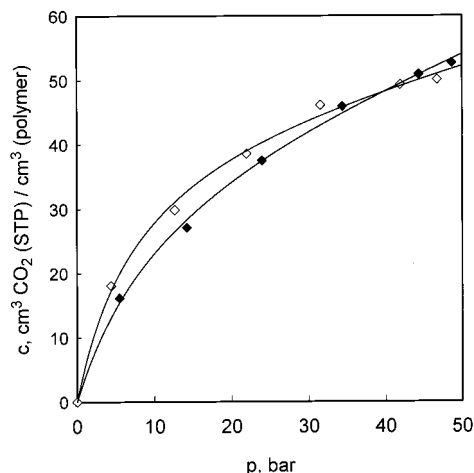

Figure 1. Sorption isotherm of CO_2 in PEI (◆) and PES (◇) at 25 °C. Symbols are experimental values; lines represents a dual-mode sorption model fit.

dioxide was quickly released from the pressure vessel (within 1 s). After removing the gas-saturated polymer film from the pressure vessel, the sample was immersed in a glycerol bath maintained at the desired foaming temperature. All samples were immersed for 30 s (foaming time). The foamed samples were next quenched in an ethanol/water (1 + 1) mixture, and washed in ethanol for a least 1 h. The washing procedure in ethanol was performed to remove adhesive glycerol traces and does not have any effect on the morphology of the foam. Subsequently, the samples were dried under vacuum (Heraeus VT 6060M in combination with an Edwards RV3 rotary vane pump) at 30 °C for 24 h to remove traces of ethanol and water. A more detailed description of the process and the influence of the process variables is given elsewhere.[3]

2.4. Foam Characterization. The foamed polymer films were characterized to determine their mass densities, cell densities, average cell size, and percolation properties.
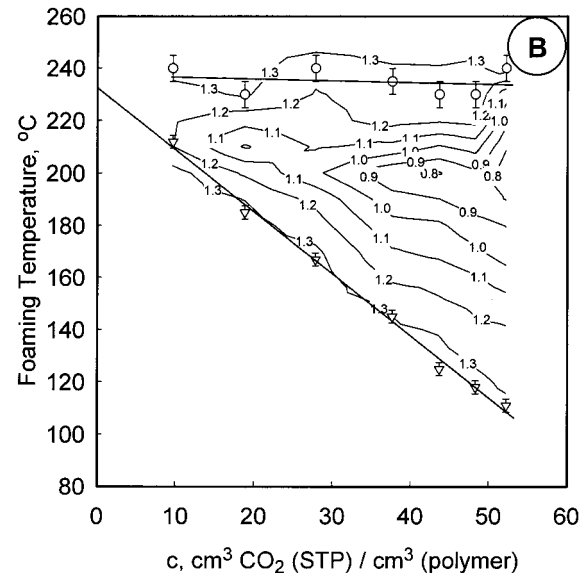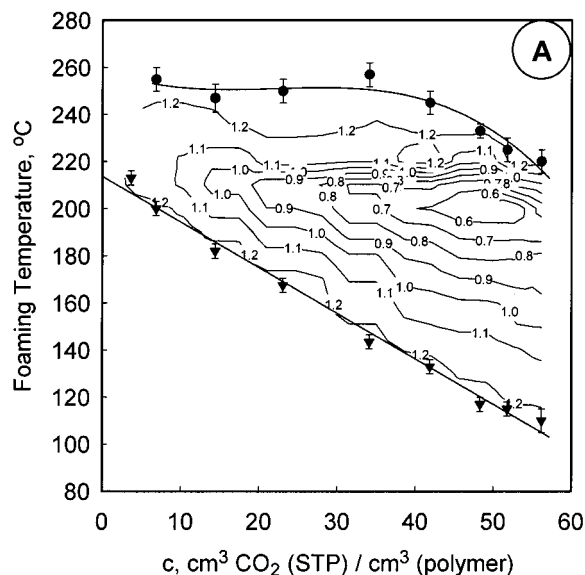
The mass densities of the foamed polymer samples were analyzed by using the flotation weight loss method (ASTM D-792) with hexane as liquid. Hexane uptake in the foamed sample could not be observed during the measurement, due to the presence of the dense skin regions covering the porous core parts. The obtained mass densities are average values of the entire polymer sample, i.e., the foamed core part including the integral dense skin. The microcellular morphologies of the foamed samples were investigated using a JEOL TM220A scanning electron microscope (SEM). The samples were freeze-fractured in liquid nitrogen and sputter-coated (Balzers/Union

Table 2. Description of the Process Variables of the Pressure Cell Technique; Foaming Experiments Are Performed with the Value or Value Ranges Given

process variable	description	value
saturation time	residence time in the CO_2 pressure vessel	120 min
saturation pressure	the CO_2 pressure in the saturation vessel	1–50 bar
saturation temp	temp in the CO_2 pressure vessel	25 °C
transfer time	the time elapsed between removing the saturated polymer sample from the pressure vessel and the heating step	20 s
foaming time	residence time of the gas saturated sample in the heating bath	30 s
foaming temp	the temp of the foaming bath	100–260 °C
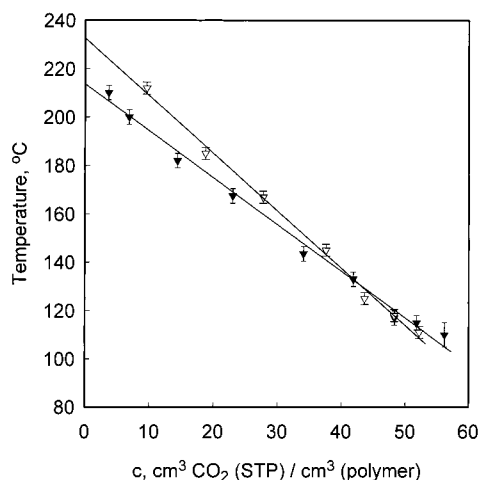
Figure 2. Glass transition temperature of PEI (▼) and PES (▽) dependent on the dissolved amount of carbon dioxide. The straight line represents a least-squares fit of the experimental data.
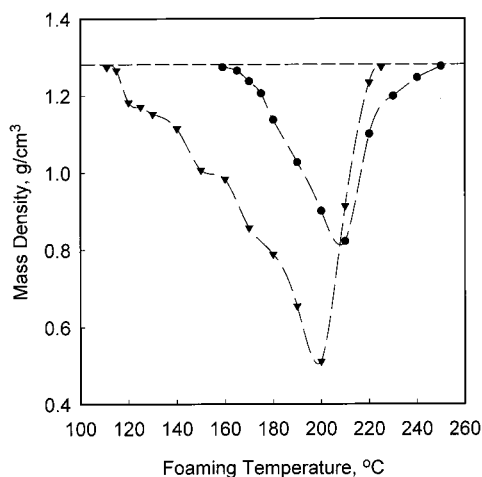
Figure 3. Mass density of PEI dependent on foaming temperature for samples saturated with 10 bar (●) and 46 bar (▼) of carbon dioxide. The dashed horizontal line represents the mass density of the pure PEI. The straight lines between the measured data points serve to guide the eye.

Figure 4. Mass density of PEI (A) and PES (B) as a function of the dissolved amount of carbon dioxide and the foaming temperature. Numbers written close to the straight lines represent the mass density of the foam in g/cm^3. The mass density contours are constructed by linear interpolation from experimental data series of nine different saturation pressures, equally distributed over the investigated concentration range. The glass transition temperature (▼, ▽) and T_{upper} (●, ○) are presented dependent on the dissolved amount of carbon dioxide. The straight line represents a least-squares fit of the experimental glass transition data.

040) with gold at an argon pressure of 0.1 Torr for 2 min at a current of 13 mA. The cell densities were determined from SEM micrographs using a procedure described previously by Kumar et al.[2] In this procedure, only the number of cells inside a window located in the center part of the foam were counted. The cell size was obtained by measuring the maximum diameter of each cell perpendicular to the skin. To obtain the average cell size, the size of at least 150 cells in the core part of the cross section of the fractured foam sample was measured. The percolation properties of the foamed films were determined using self-made gas flux modules. A detailed description of the module preparation and the measurement conditions is given elsewhere.[22] The pressure-normalized gas (helium and nitrogen) flux (P/L) through the sample is

expressed in $m^3/(m^2$ h bar). The active measurement area is calculated from the measured width of the sample and the average thickness, which was corrected for the dense unfoamed skin on the basis of SEM investigations of the cross section of
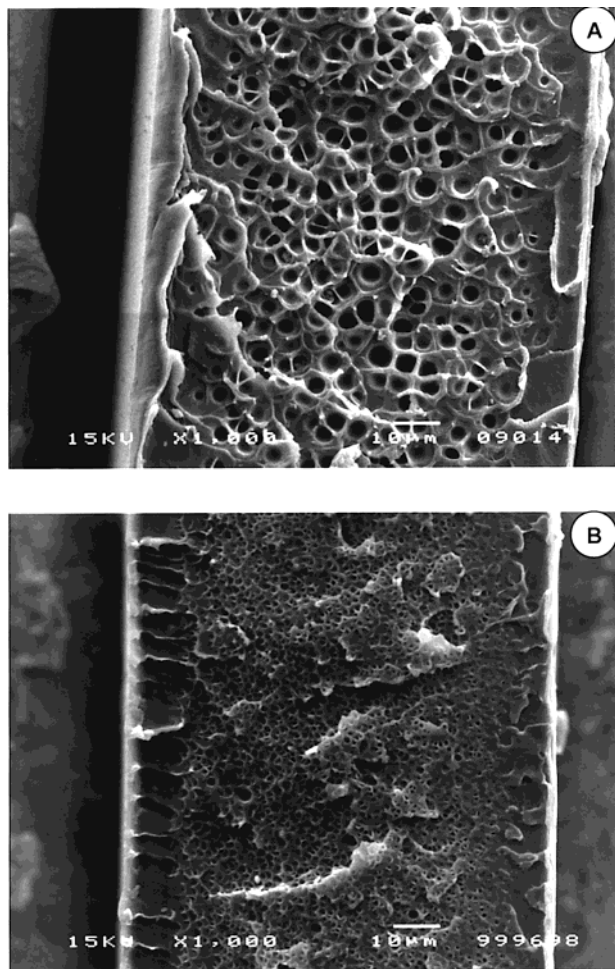
Figure 5. SEM micrographs of PEI films, which were saturated at 5 bar (A) and 30 bar (B) of carbon dioxide and foamed at 200 and 160 °C, respectively. Magnification: 1000; the white horizontal bar indicates 10 μm.

the foamed sample. The thickness of the integral skin was determined using the method described by Kumar and Weller.[27]

3. Results

Table 2 briefly summarizes the experimental conditions of which the saturation pressure (which determines the CO_2 concentration in the polymer) and foaming temperature play an important role in this work. We have used these two variables to establish a "foam window", which bounds the regions (T_{foam}, $c(CO_2)$) in which the glassy polymer/CO_2 mixture expands into a microcellular structure. We will discuss the microcellular morphology at different locations in the foam diagram and—in particular—discuss a region where the microcellular structure transforms into a nanoporous bicontinuous morphology.

3.1. Foaming Region. The region where foaming of a gas-saturated polymers occurs is fixed by (i) a lower bound temperature, T_{lower}, which resembles the glass transition temperature, $T_g(c)$, of the polymer/gas mixture at CO_2 concentration c, and (ii) an upper bound temperature, T_{upper}, where cells are destabilized by (a) diffusion of carbon dioxide out of the material and (b) the strong decrease in viscosity of the polymer ($T_{upper} > T_g(0)$).[3]

The dependence of the glass transition temperature of the polymers (PEI, PES) on the carbon dioxide concentration was determined by saturating the poly-
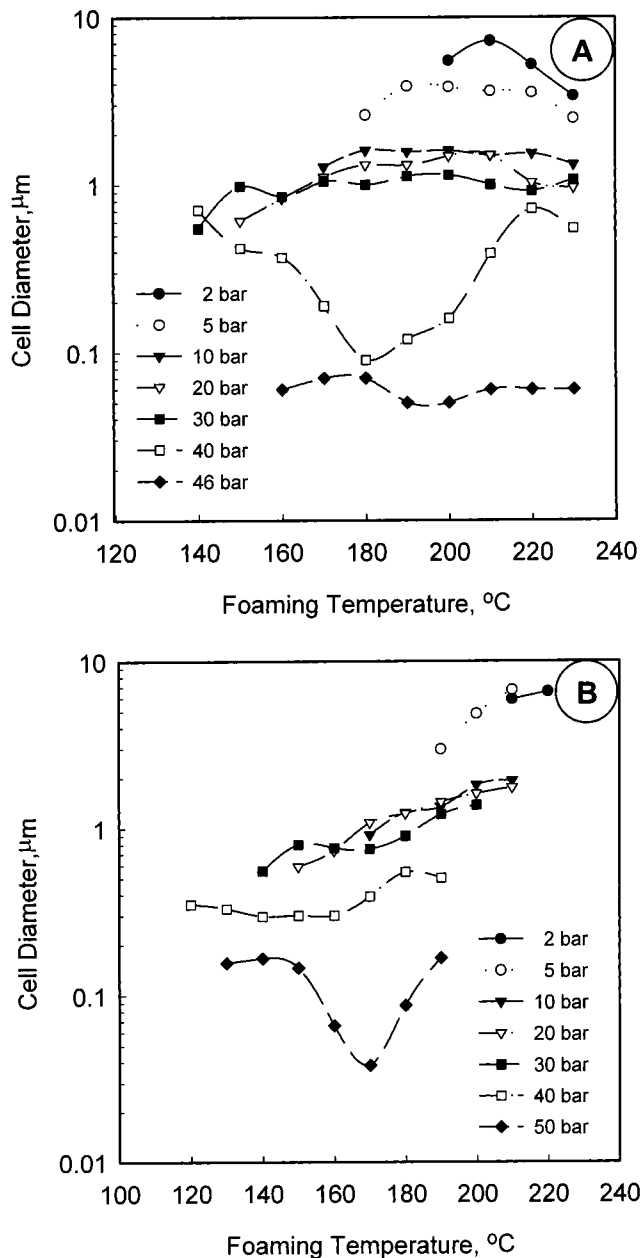

Figure 6. Average cell diameter of porous PEI (A) and PES (B) morphologies vs the foaming temperature and the carbon dioxide pressures used to saturate the samples.

mer samples at different carbon dioxide pressures (1– 57 bar) and subsequent foaming of the saturated samples at the conditions given in Table 2. The temperature at which foaming of the sample just became visible could be determined by systematically increasing the temperature of the heating bath. At this transition, the sample turns from transparent into opaque. In addition, SEM micrographs of the sample were prepared to confirm the formation of cells. The glass transition temperature was defined as the average of the two adjacent temperature values at which the transparent-to-white transition just did and did not occur. The glass transition temperatures for PES and PEI as a function of the dissolved amount of carbon dioxide are presented in Figure 2. The carbon dioxide concentrations were determined from the sorption isotherms presented in Figure 1. Concentrations at carbon dioxide pressures between 50 and 57 bar were calculated by extrapolation using the dual-mode sorption parameters presented in
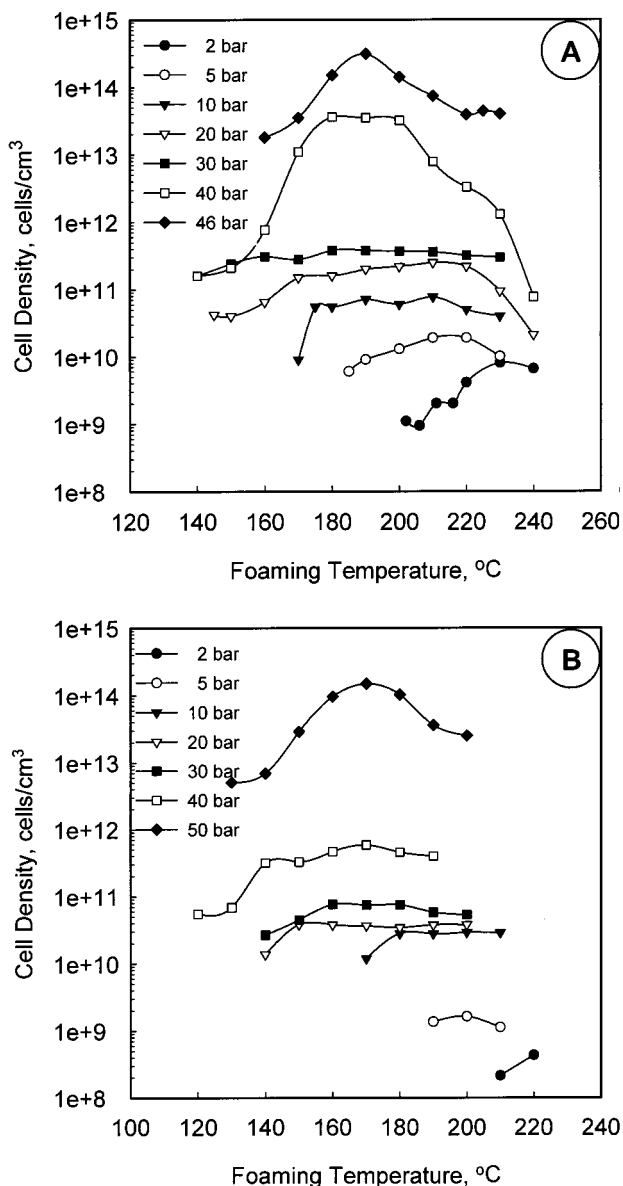
Figure 7. Cell densities of porous PEI (A) and PES (B) morphologies vs the foaming temperature and the carbon dioxide pressures used to saturate the samples.

Figure 8. Cell densities of porous PEI (A) and PES (B) morphologies vs the carbon dioxide concentration of the saturated polymers. Cell densities obtained at different foaming temperatures are included. Lines are included to emphasize the transition at approximately 47 cm^3 (STP)/cm^3 (polymer).

Table 1. Assuming a linear relation between the T_g and the dissolved amount carbon dioxide in the polymer matrix, a least-squares fit was performed. The axis intercepts in Figure 2 deviate by 2 °C for PES and by 4 °C for PEI from the T_g values obtained by DSC (Table 1).

Condo and co-workers[28] presented the concept of retrograde vitrification, which allows to predict the glass transition temperature depression of a polymer in the presence of a diluent dependent on the pressure. To obtain the concentration dependence of the T_g, one needs sorption isotherms for the whole temperature spectrum investigated. All investigated systems showed a linear relation between the glass transition temperature of the polymer/gas mixture and the dissolved carbon dioxide concentration.[29-31] As opposed to the work of Condo, our technique only requires the knowledge of one sorption isotherm.

To determine T_{upper}, experiments were performed comparable to the ones to determine $T_g(c)$; however, in this case, the foaming temperature was increased to a
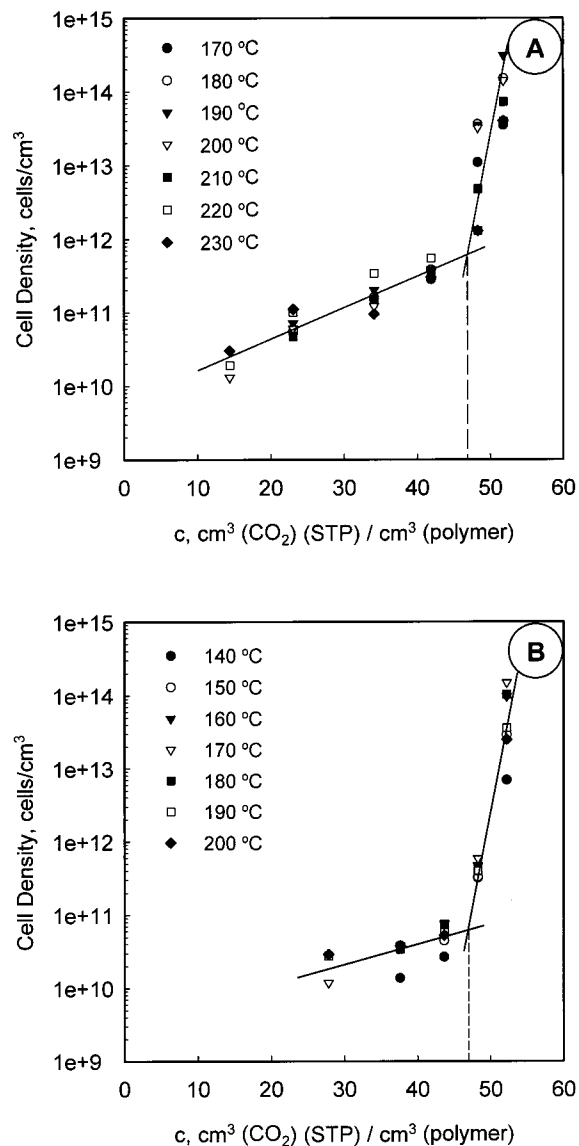
value at which the film remained transparent, while turning opaque at the previous lower temperature. In addition, SEM micrographs of the sample were prepared, and mass density measurements were performed to confirm the nonporous dense structure of the film. Two mass density data series for PEI saturated with 10 bar (23 cm^3 (STP)/cm^3 (polymer)) and 46 bar (52 cm^3 (STP)/cm^3 (polymer)) of carbon dioxide are presented in Figure 3. The upper and lower boundary temperatures are defined as the temperature where the foam density equals the density of the pure polymer, which is indicated by the dashed horizontal line. Between these two temperatures the mass density passes a minimum, which we discussed in detail in previous work.[3] We will refer to the temperature were the minimum mass density occurs as T_{max} (at this temperature a maximum in the cell density occurs). It can be observed in Figure 3 that T_{max} decreases with increasing CO_2 concentration.

The dependence of T_{lower} and T_{upper} on the dissolved carbon dioxide concentration is shown in parts A and B

Figure 9. SEM micrographs of PEI films saturated with 10 bar (A), 30 bar (B), and 40 bar (C) of carbon dioxide and foamed at 180 °C. Magnification: 1000 (A, B) and 10 000 (C); the white horizontal bar indicates 10 μm (A, B) and 1 μm (C).
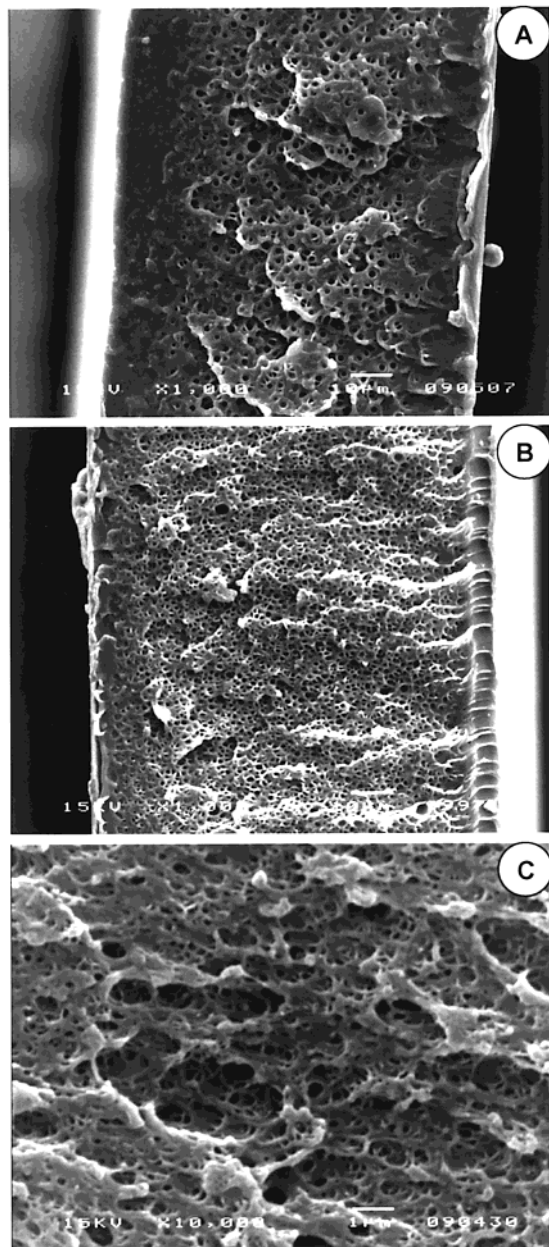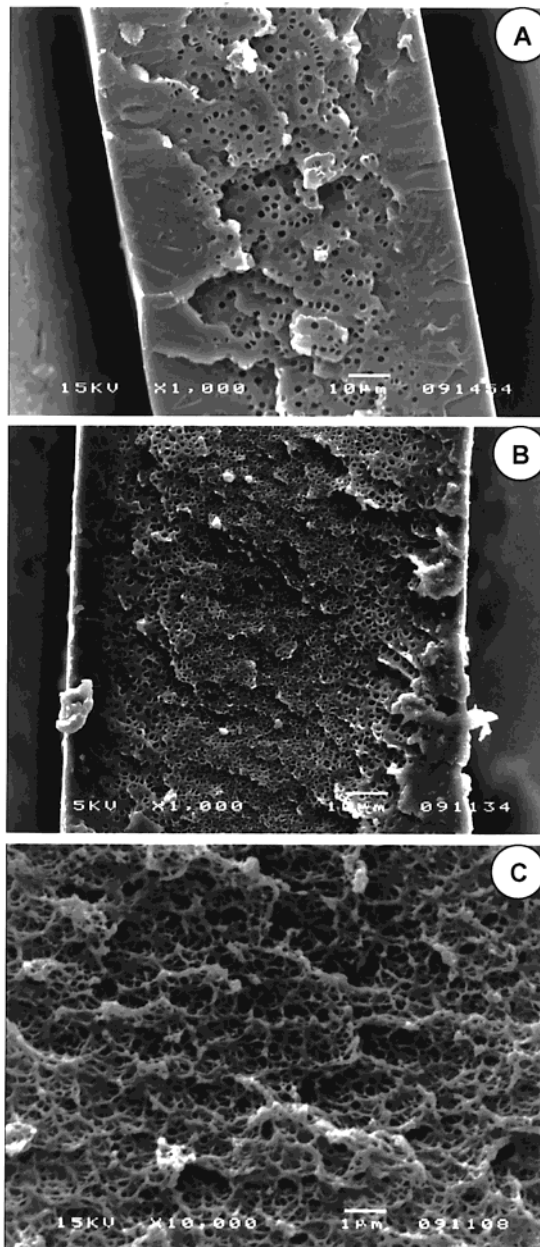

Figure 10. SEM micrographs of PES films saturated with 10 bar (A), 40 bar (B), and 50 bar (C) of carbon dioxide and foamed at 180 °C. Magnification: 1000 (A, B) and 10 000 (C); the white horizontal bar indicates 10 μm (A, B) and 1 μm (C).

of Figure 4 for PEI and PES, respectively. We will refer to the diagrams in Figure 4 as "foam diagrams" because they present the temperature and concentration envelope in which the samples expand. For PEI, T_{upper} is at approximately 250 °C in the concentration range between 8 and 40 cm^3 (STP)/cm^3 (polymer) and decreases to 220 °C at a CO_2 concentration of 58 cm^3 (STP)/cm^3 (polymer). PES shows a constant value for T_{upper} of approximately 235 °C in the investigated concentration range (10−55 cm^3 (STP)/cm^3 (polymer)). In principle, T_{upper} has to be equal to T_{lower} at zero dissolved carbon dioxide concentration ($\lim_{c \to 0} T_{upper} = T_g$). The difference between T_{upper} and the T_g of the pure polymer amounts to approximately 5 and 30 °C for PES and PEI, respectively, and is set by the time the sample is kept above its T_g; i.e., carbon dioxide loss by diffusion and polymer relaxations cause a collapse of the porous structure. Preliminary results showed that T_{upper} is in

fact a function of the material dimensions (thickness of the films) and the foaming time.

3.2. Foam Characteristics in the Foaming Region. To quantify the extent of expansion, isodensity contours are included in the foaming diagrams (Figure 4 A,B). The mass density of the foamed core region of the sample is always 20−30% lower than the reported values due to the presence of the dense skin layers. To construct the contour plots, approximately 100 samples were foamed equally distributed over the entire foaming region, bounded by T_{lower} and T_{upper}. From Figure 4 it is apparent that the isodensity lines run approximately parallel to T_{lower} in the foaming temperature range up to T_{max}. Hence, the distance from the T_g line determines the extent of expansion. Polymer relaxation and flow processes, which occur in the expansion, thus seem to obey WLF behavior occurring on the account of a temperature−concentration superposition. In contrast
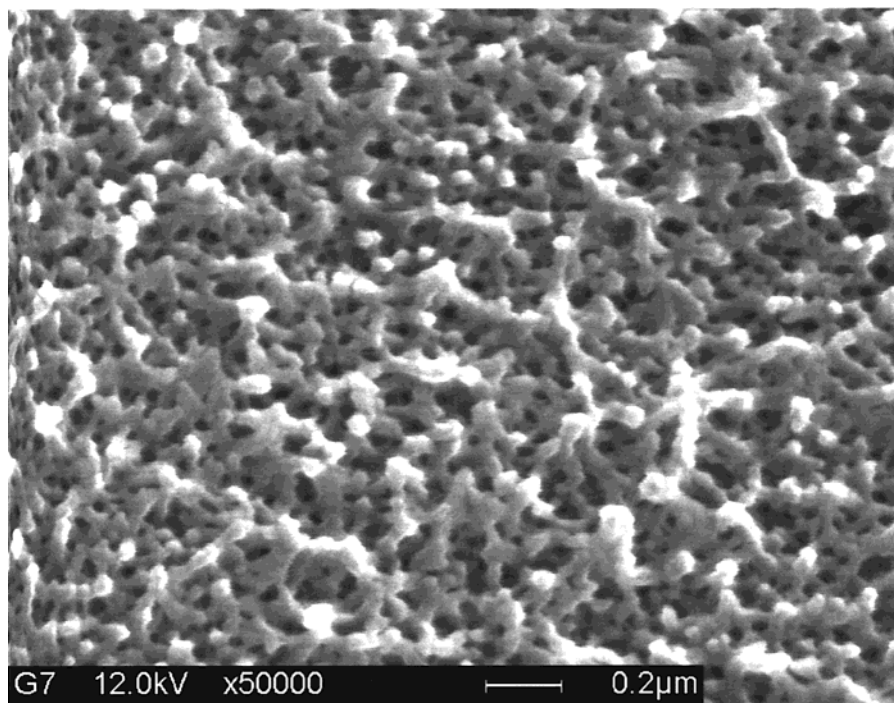
Figure 11. SEM micrograph of a PEI film saturated at 50 bar of carbon dioxide and foamed at 180 °C. Magnification: 50 000; the white horizontal bar indicates 200 nm.

to this, the isodensity lines in the temperature region between the T_{max} and T_{upper} are quite independent of the CO_2 concentration (the trend of T_{upper} is followed). This behavior occurs because CO_2 loss to the environment prevails;[3] hence, increasing the CO_2 content will not lead to significant increase of the extent of expansion.

Below T_{max}, different foam samples with identical mass density can be prepared by the proper choice of the foaming temperature and the carbon dioxide concentration in the foaming region. However, the morphology may be quite different as shown in Figure 5. Both samples exhibit the same mass density (1.05 g/cm^3); however, sample A is prepared with a saturation pressure of 5 bar and at a foaming temperature of 200 °C, whereas sample B is prepared with a saturation pressure of 30 bar and at a foaming temperature of 160 °C. The larger number of cells occurring at high carbon dioxide concentration results from the increased number of nuclei formed at elevated carbon dioxide concentration.[32]

Figure 6 shows the average cell diameters as a function of the foaming temperature and saturation pressure. As expected, low carbon dioxide saturation pressures result in large cells. PES shows average cell diameters between 0.5 and 10 μm for carbon dioxide saturation pressures between 30 and 2 bar. These are typical cell diameters one would expect for polymer/carbon dioxide systems using the pressure cell technique.[2,4,5,7−9,11,13,17,33] With PEI, however, very small cell diameters (<0.1 μm) are found at a saturation pressure of 40 bar and a foaming temperature of 180 °C and for all investigated foaming temperatures at a saturation pressure of 46 bar. Such a drastic drop in the average cell size can also be observed for PES, however, only at a slightly increased saturation pressure of 50 bar and a foaming temperature range between 160 and 180 °C. On the basis of the concave shape of the carbon dioxide sorption isotherms, such a dramatic

change in cell size is quite unexpected because the CO_2 concentration increases relatively little in the pressure range between 40 and 50 bar.

The dependence of the cell density on the foaming temperature is shown in parts A and B of Figure 7 for PEI and PES, respectively. A comparable strong increase in cell density up to 10^{14} cells/cm^3 can be observed in the same saturation pressure and foaming temperature regime where both polymers showed cell diameters below 0.1 μm. A porous polymer system with such a high cell density can no longer be defined a microcellular foam but has to be called ultra-microcellular foam.[10] To better visualize the strong increase in cell density, Figure 8 presents cell densities vs the CO_2 content of the samples. Cell densities obtained at different foaming temperatures are included. The lines indicate a general trend, which occurs at each temperature. We clearly observe that above CO_2 concentrations of approximately 45−50 cm^3 (STP)/cm^3 (polymer) cell densities rapidly increase by more than 2 orders of magnitude. This, apparently, critical CO_2 content turns out to be equal for the two polymers examined.

To illustrate the microstructural change, SEM micrographs are shown in Figures 9 and 10 for PEI and PES, respectively. The PEI samples were saturated at 10 bar (A), 30 bar (B), and 40 bar (C) carbon dioxide saturation pressure and subsequently foamed at 180 °C. The carbon dioxide saturation pressures of the foamed PES samples in Figure 10 are 10 bar (A), 40 bar (B), and 50 (C) bar, and all samples were foamed at 180 °C as well. Both series (Figures 9A,B and 10A,B) show a typical microcellular foam morphology which can easily be observed with a magnification of 1000. On the other hand, foamed PEI and PES morphologies, which were prepared at 40 and 50 bar carbon dioxide saturation pressure (Figures 9C and 10C), respectively, show very different morphologies. At a magnification of 10 000 we observe a lacy structure with openings below 200 nm in size.
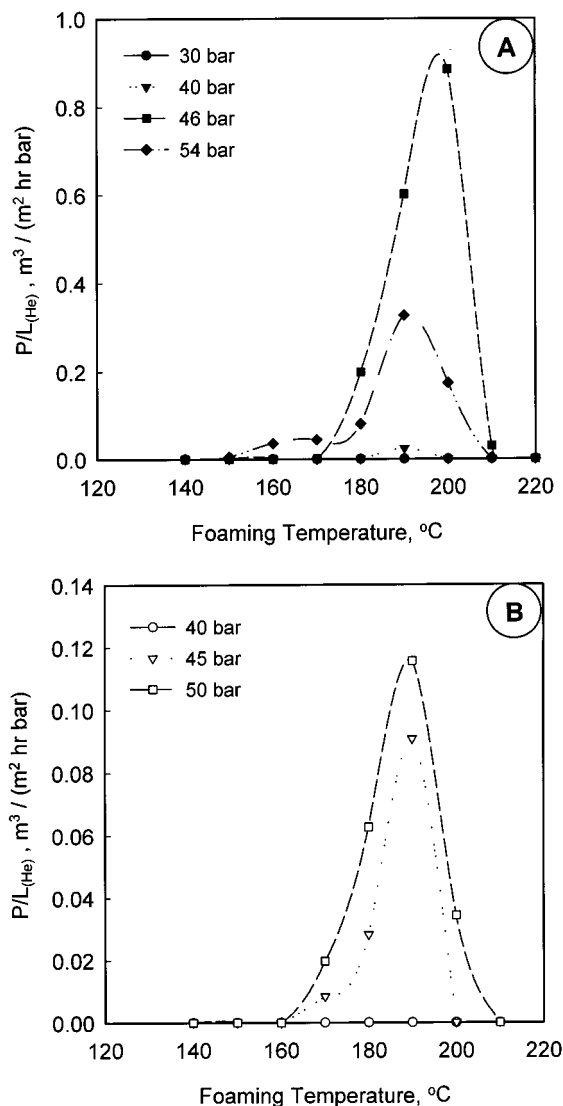
Figure 12. Normalized helium flux (P/L in $m^3 m^{-2} bar^{-1} h^{-1}$) through the cross section of PEI (A) and PES (B) foam morphologies vs the foaming temperature and the carbon dioxide pressures used to saturate the sample.

3.3. Bicontinuous Nanoporous Foams. The structural transition of foams prepared above the critical value of the CO_2 concentration reported above leads to bicontinuous nanoporous films. Figure 11 shows a bicontinuous PEI foam prepared at $T_{foam} = 190$ °C and $c(CO_2) = 54$ cm^3 (STP)/cm^3 (polymer) (50 bar of CO_2). The characteristic domain size of this sample is of the order 20−50 nm. Scanning electron micrographs of PES foams, which were prepared with a carbon dioxide concentration above 48 cm^3 (STP)/cm^3 (polymer), result in a similar morphology (not shown).

To substantiate the openness of these morphologies, gas permeation experiments were performed. Because of the presence of the dense skins, the gas flux could not be measured perpendicular to the film but had to be measured in the lateral direction through the porous morphology. Detailed information about the measurement setup is given elsewhere.[22] Both helium and nitrogen fluxes were measured of foamed PES and PEI morphologies. The normalized helium fluxes (P/L in m^3/ (m^2 h bar)) are presented in Figure 12 for PEI (A) and PES (B) foam samples prepared at different saturation pressures and foaming temperatures. It can be read from these permeation data that foamed PEI morphologies have a percolating structure and allow gas transport through the matrix if the saturation pressure is equal or above 40 bar, which corresponds to carbon dioxide concentration of 48 cm^3 (STP)/cm^3 (polymer). The foaming temperature range where these percolating morphologies are formed increase from 190 °C at 40 bar CO_2 saturation pressure up to a temperature range between 160 and 210 °C at 54 bar CO_2 saturation pressure. In Figure 12 A the helium gas flux first increases for the samples that were saturated with 40− 46 bar of carbon dioxide and next decreases again for the sample saturated at 54 bar. The smaller pore size obtained with higher values of the saturation pressure is responsible for the decrease in permeance.

The foamed PES morphologies show similar gas permeation behavior as the PEI morphologies. However, the carbon dioxide pressure required to form the bicontinuous morphology lies between 40 and 45 bar. These pressures correspond to a carbon dioxide concentration of approximately 49 cm^3 (STP)/cm^3 (polymer). The observed nitrogen fluxes (data not shown) show a similar trend as the helium flux data; however, the absolute fluxes are lower. This difference is caused by a Knudsen-type gas diffusion mechanism in the porous structure. The theoretical Knudsen separation factor for helium and nitrogen amounts to 2.65. The experimentally determined separation factors scatter within 20% of the ideal Knudsen separation factor for helium/ nitrogen (not shown). The scatter is caused by inaccuracies in the measured permeate volumes.[22] In addition to the visual inspection of scanning electron micrographs, these permeation data prove the transition from a closed-cellular structure to an open bicontinuous structure at a critical CO_2 content of approximately 48 and 49 cm^3 (STP)/cm^3 (polymer) for both polymers.

4. Discussion

On the basis of the permeation data in Figure 12, the temperature−concentration window where bicontinuous (open) structures are found may be included into the foaming diagrams (Figure 4A,B). The width of this window at a fixed value of the carbon dioxide concentration is set by two foaming temperatures, in between which gas permeation can be detected (see Figure 12). Such a window, together with the diagrams presented in Figure 4, summarizes our findings and is presented as a generalized foam diagram in Figure 13. The regions of dense (unfoamed) morphologies are represented by D_1 and D_2. The structural transition between D_1 and the microcellular region C occurs at the (lower) glass transition line. The upper temperature line (at the transition C → D_2) is assumed horizontal. In fact, this line does not represent a true *transition* because it depends on the foaming conditions (foaming time and sample dimensions). In the limit of very long foaming times or very thin samples, the line is horizontal and equals the glass transition temperature of the pure polymeric material. The region of bicontinuous morphologies, which may only be obtained above the critical CO_2 concentration c_{crit}, is denoted with B. The dashed lines schematically represent the iso-mass−density lines presented in Figure 4.

Figure 13 generally expresses the foaming behavior of high-T_g polymers with respect to the morphologies D_1, D_2, and C as shown on the basis of the present work and a previous study.[3] The region of bicontinuous
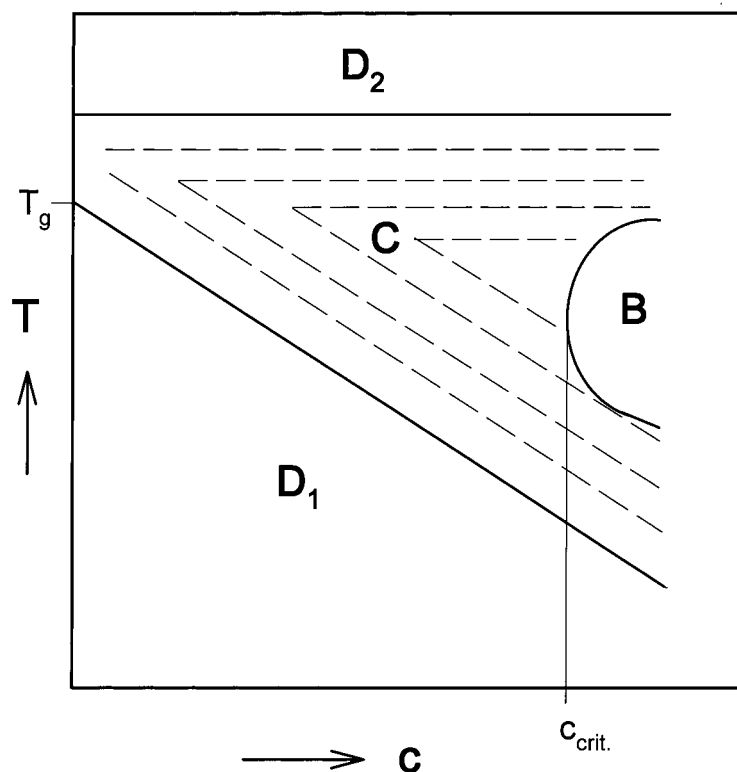
Figure 13. Generalized foam diagram, comprising the regions where dense (D_1, D_2), cellular (C), and bicontinuous (B) structures are formed. The thin lines inside the cellular region (C) represent isodensity lines.

structures has not been observed before and is marked out as a general feature as well. This region was found to occur suddenly at well-defined values of T_{foam} and $c(CO_2)$; however, it may seem ambitious to represent it as a *transition* in this diagram. Indeed, we have found a dramatic change in the porous morphologies above c_{crit} with both glassy polymers studied in this work; however, no physical basis underlying a true transition has been provided justifying our general claim of window B. Nevertheless, we argue C → B being a true physical transition on the basis of the inflection points in Figure 8A,B. If we assume that cell densities are determined by the number of critical nuclei, which grow during expansion, the lines in Figure 8 would grow continuously without any inflection occurring. Even if cells would impinge at some point a continuous trend of increasing cell density would prevail; however, then, the location of the "transition" C → B probably becomes system dependent (e.g., it would depend on how fast cells grow and whether they impinge before the structure is vitrified due to carbon dioxide loss from the dense polymer matrix). Since we do not find this, we believe that a true mechanistic change underlies the observed morphology changes. Its nature remains speculative. A comparison may be drawn between our process and the demixing of polymer/solvent systems, in which spinodal mechanisms occur. In this respect, it is important to realize that in our system demixing occurs by quick heating of an initially metastable glassy solution, and significant expansion of the structure occurs. Unfortunately, the polymer−gas demixing process is too quick to be frozen before its completion or to be followed by for example dynamic scattering methods.

Our claim of a critical carbon dioxide concentration required to prepare (open) bicontinuous structures is supported by recent work on foaming polyimides and homogeneous polyimide/polysulfone blends.[34] We have

systematically adjusted carbon dioxide concentrations in blends by varying blend ratios and have found that at the exact same value of the critical CO_2 content these structures become open.

5. Conclusions

We have reported the foaming of thin poly(ether imide) and poly(ether sulfone) films using CO_2 as physical blowing gas. The discontinuous experimental approach employed allowed to independently vary the CO_2 content of the homogeneous polymer/gas mixture and the temperature at which the actual expansion was performed. On the basis of these two parameters, foam diagrams for both polymers were presented, which mark out the regions where porous polymers are obtained. This region is bounded by (i) the glass transition temperature of the polymer/gas mixture and (ii) an upper foaming temperature limit where cells become unstable due to CO_2 loss (diffusion) and a strong decrease in viscosity of the polymer.

Within the foam diagrams, iso-mass−density lines run parallel to the line representing the glass transition temperature of the homogeneous polymer/gas mixture as long as the foaming temperatures remain well below T_{max}, at which the cell density is at a maximum. On the other hand, we find that the density of the foamed samples is independent of the carbon dioxide concentration at foaming temperatures above T_{max}.

Increasing the carbon dioxide saturation level to approximately 47 cm^3 (STP)/cm^3 (polymer) causes cell diameters to suddenly decrease below 100 nm. At the same time, the cell density increases by 2 orders of magnitude up to 10^{14} cells/cm^3. This far-reaching change in cell size and cell density corresponds to a transition from a closed cellular structure to a nanoporous bicontinuous morphology. By means of two analytical meth-

ods, viz., scanning electron microscopy and gas permeation, it could be proven that the formed foam morphologies do have a bicontinuous (open) porous structure. From SEM c_{crit} = 47 cm^3 (STP)/cm^3 (polymer) was found, whereas c_{crit} = 49 cm^3 (STP)/cm^3 (polymer) was obtained from permeation measurements. The difference falls within the experimental accuracy of our method.

The carbon dioxide concentration required to form the bicontinuous morphologies is identical for both polymers and was defined as critical carbon dioxide concentration.

References and Notes

(1) Kazarian, S. G. *Polym. Sci., Ser. C* **2000**, *42*, 78−101.
(2) Kumar, V.; Weller, J. E. *Int. Polym. Process.* **1993**, *8*, 73−80.
(3) Krause, B.; Mettinkhof, R.; Van der Vegt, N. F. A.; Wessling, M. *Macromolecules* **2001**, *34*, 874−884.
(4) Arora, K. A.; Lesser, A. J.; McCarthy, T. J. *Macromolecules* **1998**, *31*, 4614−4620.
(5) Stafford, C. M.; Russell, T. P.; McCarthy, T. J. *Macromolecules* **1999**, *32*, 7610−7616.
(6) Sumarno, T. S.; Yoshiyuki, S.; Takishima, S.; Masuoka, H. *Polym. Eng. Sci.* **2000**, *40*, 1510−1521.
(7) Kumar, V.; Weller, J. *J. Eng. Ind.* **1994**, *116*, 413−420.
(8) Blednykh, E. I.; Skripov, V. P. *Colloid J. Russ. Acad. Sci.* **1996**, *58*, 15−20.
(9) Goel, S. K.; Beckman, E. J. *Polym. Eng. Sci.* **1994**, *34*, 1137−1147.
(10) Handa, Y. P.; Zhang, Z. *J. Polym. Sci., Polym. Phys. Ed.* **2000**, *38*, 716−725.
(11) Goel, S. K.; Beckman, E. J. *Polym. Eng. Sci.* **1994**, *34*, 1148−1156.
(12) Doroudiani, S.; Park, C. B.; Kortschot, M. T. *Polym. Eng. Sci.* **1996**, *36*, 2645−2662.
(13) Baldwin, D. F.; Shimbo, M.; Suh, N. P. *J. Eng. Mater. Technol.* **1995**, *117*, 62−74.
(14) Nayak, N. C.; Tripathy, D. K. *Cellul. Polym.* **2000**, *19*, 271−286.
(15) Murray, R. E.; Weller, J. E.; Kumar, V. *Cellul. Polym.* **2000**, *19*, 413−426.
(16) Lee, K.-N.; Lee, H.-J.; Kim, J.-H. *Polym. Int.* **2000**, *49*, 712−718.
(17) Kumar, V. *Cellul. Polym.* **1993**, *12*, 207−223.
(18) Throne, J. L. *Thermoplastic Foams*; Sherwood Publisher: Hinckley, OH, 1996.
(19) Huang, Q.; Seibig, B.; Paul, D. *J. Membr. Sci.* **1999**, *161*, 287−291.
(20) Huang, Q.; Seibig, B.; Paul, D. *J. Cellul. Plast.* **2000**, *36*, 112−125.
(21) Rodeheaver, B. A. Open-Celled Microcellular Thermoplastic Foam. M.S. Thesis, Georgia Institute of Technology, 1999.
(22) Krause, B.; Boerrigter, M. E.; Van der Vegt, N. F. A.; Strathmann, H.; Wessling, M. *J. Membr. Sci.* **2001**, *187*, 181−192.
(23) Koros, W. J.; Paul, D. R.; Rocha, A. A. *J. Polym. Sci., Polym. Phys. Ed.* **1976**, *14*, 687−702.
(24) Koros, W. J.; Paul, D. R. *J. Polym. Sci., Polym. Phys. Ed.* **1976**, *14*, 1903−1907.
(25) Bos, A. High Pressure CO_2/CH_4 Separation with Glassy Polymer Membranes. Ph.D. Thesis, University of Twente, 1996.
(26) Koros, W. J.; Paul, D. R. *J. Polym. Sci., Polym. Phys. Ed.* **1976**, *14*, 675.
(27) Kumar, V.; Weller, J. E. *Polym. Eng. Sci.* **1994**, *34*, 169−173.
(28) Condo, P. D.; Sanchez, I. C.; Panayiotou, C. G.; Johnston, K. P. *Macromolecules* **1992**, *25*, 6119−6127.
(29) Condo, P. D.; Johnston, K. P. *Macromolecules* **1992**, *25*, 6730−6732.
(30) Condo, P. D.; Johnston, K. P. *J. Polym. Sci., Polym. Phys. Ed.* **1994**, *32*, 523−533.
(31) Condo, P. D.; Paul, D. R.; Johnston, K. P. *Macromolecules* **1994**, *27*, 365−371.
(32) Zettlemoyer, A. C. *Nucleation*; Marcel Dekker: New York, 1969.
(33) Wessling, M.; Borneman, Z.; Boomgaard, A. Van den; Smolders, C. A. *J. Appl. Polym. Sci.* **1994**, *53*, 1497−1512.
(34) Krause, B.; Diekmann, K.; Van der Vegt, N. F. A.; Wessling, M., to be published.